An Effective Supramolecular Mg(II)-Metallohydrogel based Non-Volatile Memory Device with Supreme Endurance

Arpita Roy and Soumya Jyoti Ray[a]

Department of Physics, Indian Institute of Technology Patna, Bihar-801106, India.

[a]ray@iitp.ac.in

Abstract

Traditional computer systems are becoming unable to handle the needs of upcoming data-intensive applications. Resistive random access memory devices (RRAM), which offers a potential advancement in existing computing design, are preferred as promising alternatives for the application in neuromorphic computing. In this work supramolecular Mg(II)-based metallohydrogel, referred as Mg@5AP was synthesized by 5amino 1pentanol as Low Molecular Weight Gelator (LMWG) at normal temperature. From scanning and transmission electron microscopy (FESEM and TEM), we observed a unique network of rectangular, pebble-like structures within Mg@5AP. From Fourier-transform infrared (FT-IR) spectroscopy, we identified organic compounds which were present in this metallohydrogel. Here, we prepared schottky diode with the configuration of metal-semiconductor-metal using Mg@5AP. To investigate its charge transportation property, we developed Mg@5AP based RRAM device with lateral and vertical configurations which exhibited a bipolar resistive switching behavior. Behind this switching mechanism, formation and rapture of conduction filament between two electrodes were responsible. It demonstrated impressive endurance with a high ON/OFF ratio (~120) upto 5000 switching cycles. Here, 2×2 crossbar array based on Mg@5AP was also prepared to demonstrate logic gate operation. In this work, it was confirmed that it worked as in-memory computing where storage and processing both were occurred simultaneously. Therefore, it provided a cost-effective and environmentally friendly alternative to conventional heavy metal-based memory systems for high-performance data storage.

Keywords: Supramolecular Mg(II) metallogel, Schottky Diode, Resistive Switching, Conduction filament, Neuromorphic computing.
Received 30 January 2025; First Review 8 April 2025; Accepted 18 April 2025.

*** Address of correspondence**
Soumya Jyoti Ray
Department of Physics, Indian Institute of Technology Patna, Bihar-801106, India.

Email: ray@iitp.ac.in

How to cite this article
Arpita Roy and Soumya Jyoti Ray, An Effective Supramolecular Mg(II)-Metallohydrogel based Non-Volatile Memory Device with Supreme Endurance, J. Cond. Matt. 2025; 03 (02): 107-113.

Available from:
https://doi.org/10.61343/jcm.v3i02.104

Introduction

A supramolecular metallogel [1-3] refers to a gel designed by the self-assemble of metal ions or metal by non-covalent interactions such as H-bonding, π-π stacking, van der Waals force. Unlike traditional gels formed by covalent bonds, supramolecular gels are held together by these reversible interactions, allowing for dynamic and versatile properties. Molecules in these gels organize themselves into a 3d network, trapping solvent or liquid within this structure. Besides this, low molecular weight gelator (LMWG) is a small molecule which is capable of forming gels by self-assembly at relatively low concentrations. They have the unique ability to form gel networks through non-covalent interactions. In this work, 5amino 1pentanol serve pivotal role as a LMWG within this metallohydrogel. There are lots of applications of this metallogel in diverse fields such as sensors, memory gadgets, catalysis, semiconducting diodes, magnetic performance etc.

Here, we have successfully synthesized a novel mechanically stable metallogel using 5amino 1pentanol only as single LMWG and Mg(II) metal ions sourced in N, N-dimethylformamide solvent. Notably, we accomplished this without any requirement of additional supporting ligands. This work mainly highlights the capability of metallogels to contribute as a crucial component in constructing metal-semiconductor (MS) junction devices exhibiting Schottky barrier properties and non-volatile memory device functionalities [4-6]. Owing to its compatibility with CMOS design, simple configuration, cost-effectiveness, low power consumption [4], fast data transfer speed, stability [7], reliability [8], resistive random-access memory (RRAM) technology [9-13] is advantageous for upcomimg generation memory design, and also neuromorphic [14-15] and in memory computing [16,17]. Recently, researchers have already demonstrated switching performance of transition metal oxide-based RRAM device [18-21]. Nevertheless, researchers seek alternative devices

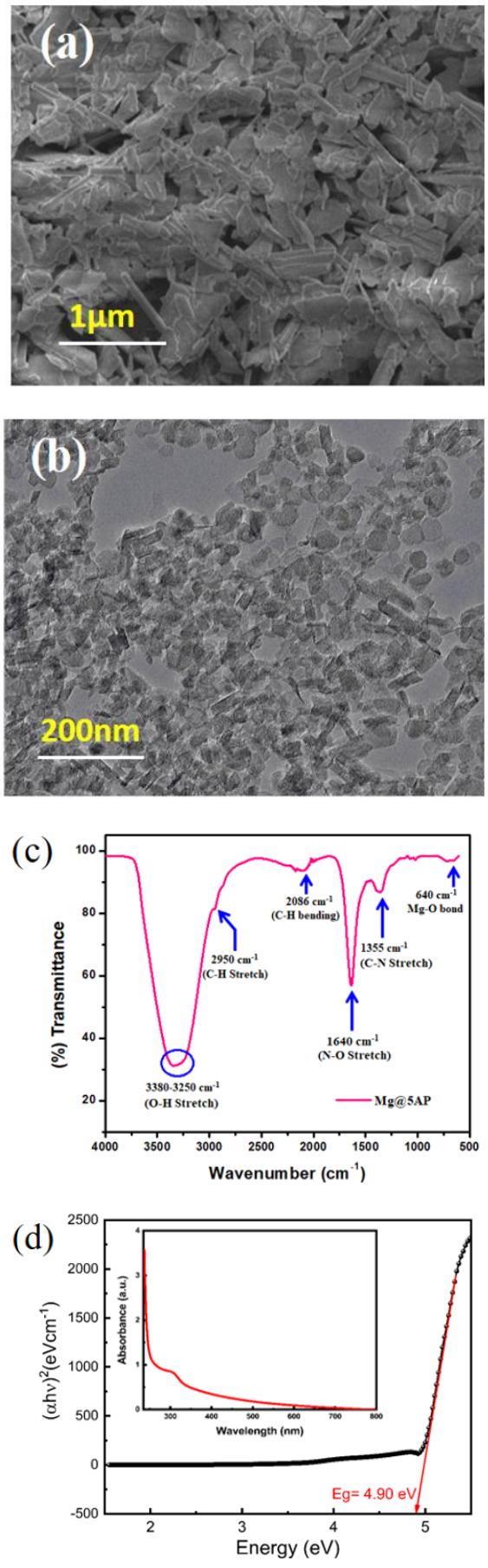

Figure 1: (a) FESEM pattern of Mg@5AP metallogel, **(b)** TEM image of Mg@5AP metallogel, **(c)** FT-IR spectra of Mg@5AP, **(d)** Tuac's plot for Mg@5AP metallogel and UV-Vis absorption spectra (inset).

to enhance the switching performance, with metallogel presenting potential due to their semiconducting behavior and capacity for device fabrication. Our research begins by introducing the key synthetic strategies and characterization methods for Mg(II) based metallogel. Next, it provides an overview of this metallogel-based memristive material and their commonly used switching mechanisms. Moreover, flexible electrical and optoelectronic devices with memory, sensing, and optical detecting capabilities can be made by developing metallohydrogel-based RRAM structures on flexible substrates.

However, memristors hold significant applications in designing logic gate circuits because of their nonlinearity and non-volatility [22-23]. This work provides a clear outline of logic gate and assesses their part in the memory related application. Here, we have demonstrated the applications of this device in memristor arrays for logic implementation. The work also explores recent advancements in metallogel based memristor for neuromorphic computing, data storage, artificial synapses, logic circuit etc. At last, it discusses the experiments, development trends, and future perspectives by offering a guidance for development of efficient supramolecular Mg(II)-metallogel based memristors and their applications in information technology.

Methodology

1. Material

Magnesium Nitrate Hexahydrate and 5amino 1pentanol were used to synthesize the metallohydogel (Mg@5AP). Both chemicals were utilized in their as-received state without additional purification. Double-distilled water was consistently used in all experiments.

2. Preparation of Mg(II) metallohydrogel (Mg@5AP)

A 500 µL clear solution containing $Mg(NO_3)_2 \cdot 6H_2O$ (0.256 g, 1 mM) and 500 µL of 5amino 1pentanol are rapidly combined within 5 mL glass vial at normal temperature. Following a gentle shaking of this vial, a white-coloured Mg@5AP is instantly created.

3. Fabrication of device

We created a device with a Schottky diode structure with lateral configuration such as ITO /Mg@5AP/ITO (Device 1) (Fig. 2(a)) to show their electrical behavior in this study. To create MS junction, we have drop-casted Mg@5AP metallogel on an ITO (Indium Tin Oxide) substrate. ITO is a perfect material for photo-excitations because it is both an excellent electrode and transparent substance optically in visible area. We also fabricated two RRAM devices with vertical configurations of ITO/Mg@5AP/Cu (Device 2) (as shown in Fig. 3(a): inset) and Cu/Mg@5AP/Cu (Device 3)

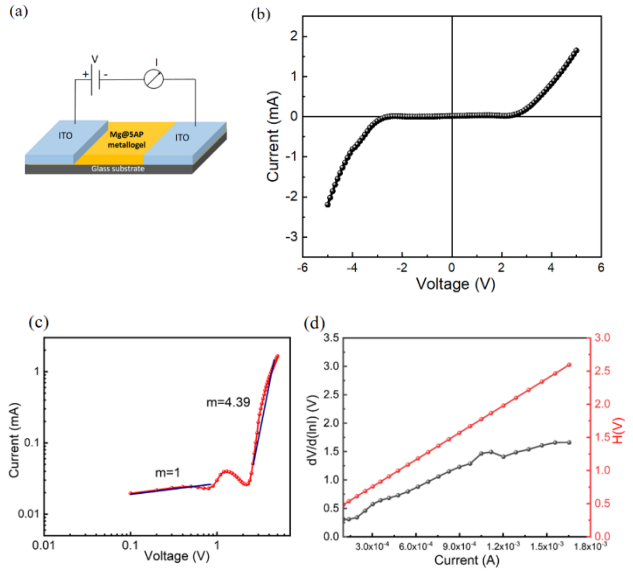

Figure 2: (a) Representation of Mg@5AP based-device-(ITO/Mg@5AP/ITO), **(b)** IV curve for same device on linear scale, **(c)** IV curve on logarithmic scale, **(d)** H versus. I graph; dV/d(ln I) versus. I graph for same device.

(as shown in Fig. 4(a): inset) to develop RRAM device. In both configurations, Mg@5AP was deposited onto the substrate (bottom electrode). Then, the topmost electrode (Cu) is kept onto the material for making this device.

Outcomes

1. Structural Analysis of Mg@5AP metallohydrogel

FESEM and TEM images of Mg@5AP metallogel shows a distinctive hierarchical network of flake-like patterns which are shown in Fig.1 (a,b) respectively. EDX mapping further corroborates the composition of the network which confirms the existence of carbon (C), oxygen (O), nitrogen (N), magnesium (Mg) arising from $Mg(NO_3)_2$, 5-amino-1-pentanol and DMF molecules (as shown Fig.S1).

2. Analysis of Fourier Transform Infrared Spectra (FT-IR) of Mg@5AP metallohydrogel

FT-IR spectra of the Mg@5AP provides insights into the primary interactions between 5amino 1pentanol and the source of Mg(II) in this gel formation (Fig. 1(c)). Within this spectrum, broad peaks within 3380-3230 cm^{-1} correspond to O-H- stretching, while peaks at 2950 cm^{-1} and 2086 cm^{-1} are corresponded to C-H- stretching vibrations, C-H- bending vibrations respectively. Additionally, 1640 cm^{-1} and 1355 cm^{-1} correspond to N-O- stretching and C-N stretching respectively. Furthermore, to understand the robustness of the interaction between 5amino 1pentanol and the solution of magnesium nitrate, an observable peak at 640 cm^{-1} is identified (Fig. 1(c)). This specific peak signifies the presence of Mg-O bonds, providing further confirmation of the metallohydrogelation process.

3. Optical characterization

To establish the optical behaviour of the synthesised Mg@5AP, Ultra-violet-visible spectra (inset of Fig. 1(d)) were analysed using the Tuac's Plot, as shown in Fig. 1(d). A wavelength range from 250 nm to 800 nm was taken for the measurement. From the UV-vis spectrum, we used Tauc's equation (1) to estimate the direct bandgap (E_g) of this metallogel Mg@5AP:

$$(\alpha h\nu)^n = A\,(h\nu - E_g) \qquad (1)$$

Where α = Coefficient of Absorption, E_g = band gap, h = Planck's constant, and ν = frequency of the light. In the processes, "n" is the constant (n=2); "A" is also constant (A=1). We determined E_g, which is 4.90 eV, by ranging the linear area of the plot $(\alpha h\nu)^2$ versus hν (Fig. 1(d)) up to the region where there is no absorption. This type of high bandgap materials typically absorb less in the visible spectrum which makes the device more optically transparent. This is useful in transparent electronics, UV photodetectors, and solar cells with wide-spectrum coverage. They are often more thermally stable, which could make the device suitable for use in high-temperature or harsh environmental conditions. This also leads to lower leakage currents and better control over charge transport, which is beneficial for low-power electronic applications.

4. Electrical Characterization of Device

In order to provide an accurate measurements of the material's semiconductor nature, the charge transportation properties of Mg@5AP based RRAM devices are done by two-probe arrangements. I-V curve of ITO/Mg@5AP/ITO (device-1) in the voltage (-5 V to +5V) is displayed in Fig. 2(b) on linear scale. In both +ve and -ve polarity, the current increased with voltage beyond this region. By using thermionic emission theory (TE Theory), Schottky diode parameters are derived from the IV curve. Cheung [24] proposed this technique. The equations (2-3) are used to evaluate the measured IV curve:

$$I = I_0\, exp\left(\frac{qV}{\eta k_B T}\right)\left[1 - exp\left(\frac{-qV}{\eta k_B T}\right)\right] \qquad (2)$$

$$I_0 = A\,A^*\,T^2\,\exp\left(\frac{-q\phi_B}{k_B T}\right) \qquad (3)$$

Here, I_0 = Current of saturation; q = Charge of electron; k_B = Boltzmann Constant; T = Temp; V = Voltage; Φ_B = Height of barrier potential; A = Effective Area of Diode; R_S = Resistance in series; η = Factor of ideality; A* = Effective Richardson Constant (~32 $AK^{-2}cm^{-2}$).

Here, log(I) versus. log(V) graph is plotted (Fig. 2(c)) to define the conduction mechanism. At lower voltage zone, it

followed Ohomic conduction with the slope of 1; but in higher voltage region, it followed Space-Charge-Limited Conduction mechanism with the slope of m=4.39.

$$\frac{dV}{d(\ln I)} = \left(\frac{\eta k_B T}{q}\right) + IR_S \quad (4)$$

$$H(I) = V - \left(\frac{\eta k_B T}{q}\right) \ln\left(\frac{I}{AA^* T^2}\right) \quad (5)$$

$$H(I) = IR_S + \eta\phi_B \quad (6)$$

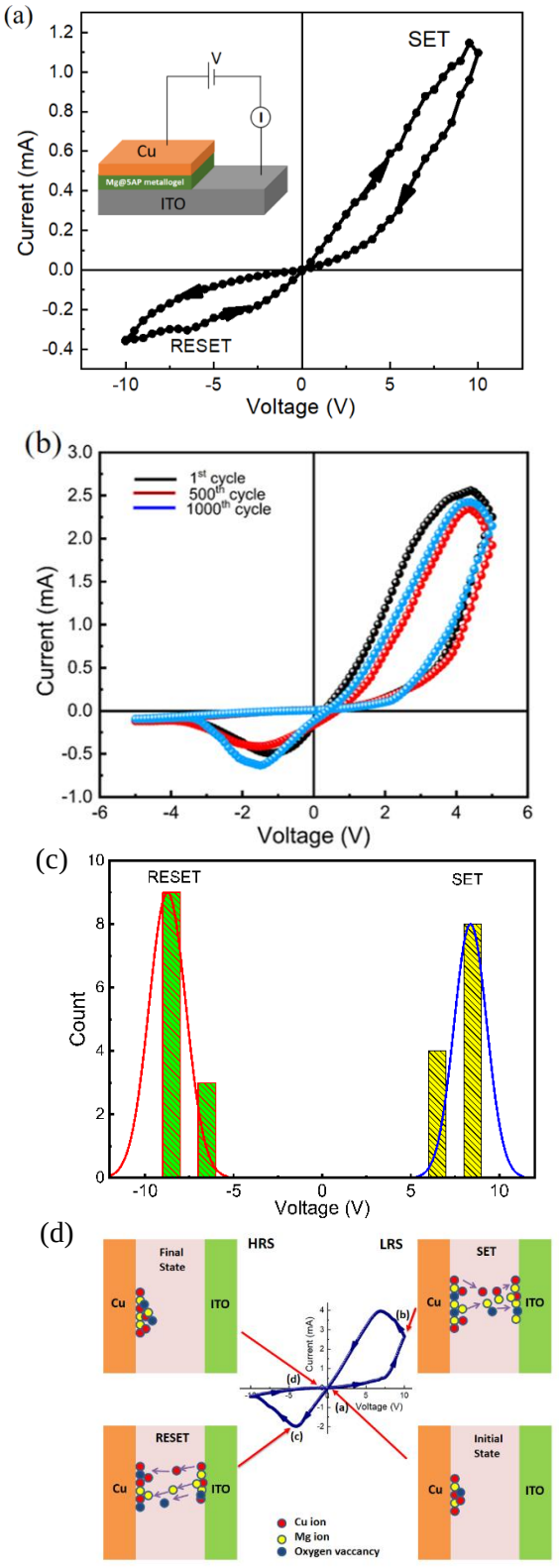

Figure 3: (a) Diagram of ITO/Mg@5AP/Cu device (inset), with IV curve of this device in linear scale, **(b)** I-V characteristics upto 1000th cycle, **(c)** Voltage distribution function of SET and RESET voltage for multiple devices, **(d)** Conductive filament model of this device. The following places have been located using the *I–V* curve: (a) The ions move towards the intermediate layer after applying a positive voltage of 0.5 V; (b) at 9.94 V, the Cu ions, Mg ions, and oxygen vacancies produced a conducting filament-type structure; (c) at −4 V, all the ions including Cu ions, Mg ions return to the top electrode; and (d) at −0.5 V, all of the ions are gathered at the top electrode and switched into HRS.

The value of R_S; η; and Φ_B are determined from equations (4-6). Here, dV/d(ln I) versus I and H versus I were plotted to obtain the constraints of device 1, as shown in Fig. 2(d). The intercept of H versus. I graph was used to define the height of barrier, and the intercept of this graph was used to get the ideality factor (η). We determined the ideality factor (η) which is 13.497 that is greater than the actual value. The high ideality factor may arise from interface traps, surface roughness, or imperfect contact between ITO and this metallohydrogel, leading to non-uniform potential barriers. This discrepancy of it could be produced by the interfacial resistance, presence of interface states and the impurities in the Schottky barrier itself. The value of (ϕ_B) which is 0.0258 eV, is established for device-1. Therefore, these characteristics such that a lower height of barrier potential and greater value of ideality factor are important for developing Schottky diode. The slope of the graph of dV/d(ln I) versus I and H versus I (Fig. 2(d)) was also calculated to obtain the value of the resistance in series (~1358.04 Ω). This diode can be useful for making different electronic devices.

To analyze the resistive switching behavior (RS) of ITO/Mg@5AP/Cu (device-2) we have fixed the Compliance Current (CC) at 10 mA before starting the experiments. IV curve of this device is displayed on linear scale in Fig. 3(a). The applied voltage follows this sequence: 0V→10V→-10V→10V. This IV characteristics display a proper hysteresis that is a signature of memristive behaviour. Firstly, the current rises linearly. When applied voltage increases, the IV graph demonstrates a nonlinear nature above a certain voltage of 5.85V and then the current increases rapidly. Then the device is switched to a Lower Resistance State (LRS) from a Higher Resistance State (HRS), as specified by SET voltage (V_{SET} = 10V) and it stays in ON state. In the negative zone, the voltage decreases, it goes into OFF state and the current decays quickly. After a reverse cycle, it increases until it goes to an LRS. When V_{RESET} is -9.98V, it goes to the HRS. A negative voltage is necessary to restore a device to its initial state, this is essential evidence of the bipolar RS behavior of this device. We have again examined the entire IV curves for device 2 up to 1000th cycles and observed that there isn't much more variation in the current value up to the 1000th

cycle (Fig. 3(b)). Therefore, metallohydrogel-based RRAM devices are reliable and do not degrade upto 1000th cycles. We have also plotted voltage distribution function of SET and RESET voltage for multiple devices as shown in Fig. 3(c).

In the semiconducting layers of device 2, conducting filaments [25] are formed and the main reason behind this filament formation is the migration of copper ions, oxygen vacancies and Mg ions (Fig. 3(d)). We can easily explain the change from the HRS to LRS by the development and breaking of Cu conductive filaments. As we already know that their chemical formula is Cu→ Cu^{2+} + e^{-}. Cu ions may go towards the electric field and then they are ionized. When we apply +ve voltage, Cu^{2+} ions, oxygen vacancies and Mg ions travel to the in-between layer. The device changes to LRS from HRS during SET process and then concentration of all ions will go to the bottommost electrode. Then the device residues in the same state until a negative voltage is applied to the electrode during RESET. When a negative voltage is supplied, it enters the HRS. At the end of the procedure, all ions return to the topmost electrode.

Fig. 4(a) shows I-V curve of device 3 (CuMg@5AP/Cu) with two states (V_{SET} = 7.17V and V_{RESET} = -9.98V). To understand its mechanism, IV curve is fitted in a log scale in SET process (Fig. 4(b)). In the lower voltage range of 0V to 2V, the current is seen to vary linearly with slope of 1.09 and from 2V to 5V, the slope of m= 1.39 that means it shows Ohmic conduction. But in the higher voltage range of 5V to 10V, it follows a SCLC mechanism with slope of 4.10. We have also measured endurance up to 5000 multiple cycles (Fig. 4(c)). The average ON/OFF ratio of this device, which is to be around 120, shows highly robust switching behaviour. This indicates that there won't be any degradation in the device's memory response, that is advantageous for practical application in designing memory circuit. As seen in Fig. 4(d), we have also conducted retention test for devices 3 for up to 10^7 s. Device 3's switching process is reliable for a maximum of 10^7 seconds. Additionally, we have noticed that the device's ON/OFF ratio is approximately 90. It is concluded that these devices have no degradation in data storage for up to 10^7 seconds. We have also described the electrical performance of different RRAM devices as shown in Table 1.

In our study, we have also designed Mg@5AP based 2×2 cross-bar array and demonstrated logic gate operation. We have placed our sample at the interception of two Cu electrodes as shown in Fig. 5. Mg@5AP based RRAM devices are defined as A; B; C; and D.

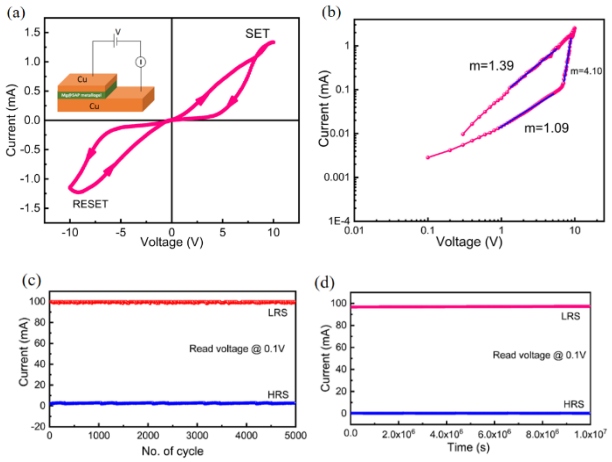

Figure 4: (a) Diagram of Cu/Mg@5AP/Cu-device (inset), with its IV curve on linear scale, **(b)** I-V Curve on a log scale, **(c)** Endurance test of same device, **(d)** Retention test of this device.

Table 1: Comparative studies of different RRAM devices.

RRAM device	Endurance (cycles)	Retention (s)	ON/OFF ratio	Ref.
Al_2O_3/ZnO- based RRAM	10^4	10^4	10^5	[26]
Pt/AlO_X/ZnO/Ti	10^3	10^4	10^2	[27]
Pt/HfO_2/TiO_X/Pt	100	10^4	10^2	[28]
Graphene/HfO_2/TiN	10^3	10^4	10^2	[29]
hBN/AlO_X/TiO_X/ITO	100	10^4	10^2	[30]
Cu/Mg@5AP/Cu	5000	10^7	10^2	This work

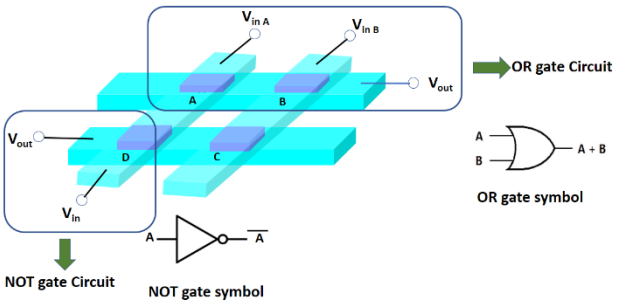

Figure 5: Circuit diagram of Logic gate

In case of OR gate, when there is zero voltage at device A and B, that means both are in "0" state, then V_0 (Output voltage) = 0.09V mentioned to as "0" state. When 5V is applied to A and 0V is provided at B, then V_0 = 4.89V referred to as "1". Similarly, when 0V is provided to A and 5 V is applied to B, then V_0 = 4.86 V which is also mentioned to as "1". When we apply 5 V to the both A and B, then V_0 = 4.85V corresponds to "1". The truth table of OR gate is given in Table 2.

Table 2: OR gate Truth Table.

$V_{A\ input}$	$V_{B\ input}$	V_0	State
0 Volt	0 Volt	0.09 Volt	0
5 Volt	0 Volt	4.89 Volt	1
0 Volt	5 Volt	4.86 Volt	1
5 Volt	5 Volt	4.85 Volt	1

Similarly, we have also designed NOT gate using device-D and it obeys NOT gate truth table (Table 3).

Table 3: NOT gate Truth Table.

V_{input}	V_0	State
0V	4.83V	1
5V	0.06V	0

The current configuration can be further stretched to incorporate larger-cross-bar arrays in order to accomplish more intricate logic and computation processes. This can be the basis for in-memory computing, as demonstrated here, in which regulating and storing information are done at the same circuit level. Thus, a variety of engineering approaches based on the principles of integrated circuit can be investigated through the use of memristor based crossbar arrays in logic gate.

Conclusion

Mg@5AP metallohydrogel was effectively synthesized by rapidly mixing of $Mg(NO_3)_2{\cdot}6H_2O$ with 5-amino-1-pentanol in an aqueous medium at normal temperature. Microstructural investigations from FESEM and TEM exposed the pebble-like structure of this gel, while FTIR spectra characterized intermolecular interactions. Tauc plot showed the semiconducting behaviour of this gel. MS junction-based Schottky diode was developed using this Mg@5AP metallogel. Moreover, ITO/Mg@5AP/Cu and Cu/Mg@5AP/Cu devices are fabricated, both exhibiting bipolar RS behavior. This behavior was recognized to the development and rapture of conduction filaments. Impressively, they demonstrated non-volatile switching behaviour, maintaining an excellent ON/OFF ratio (~120) over 5000 multiple cycles without any electrical degradation. Recent research suggests that this gel is a promising candidate for memory device applications due to its strong RS behavior and significant ON/OFF ratio. It is also a desirable choice for applications in neural circuit design, neuromorphic computing and also for the development of flexible electronic devices by utilizing the thin films of Mg@5AP for cutting-edge technology due to its stable switching performance and adaptable functionalities.

Acknowledgements

Arpita Roy acknowledges the financial support from UGC, India through UGC-NET scholarship.

Conflict of Interest

The authors declare no conflict of interest.

Data Availability Statement

The data that support the findings of this study are available from the corresponding author upon reasonable request.

Author Information

ORCID
Arpita Roy: 0009-0005-9649-3608
Soumya Jyoti Ray: 0000-0002-4640-708X

References

1. R. Kuosmanen, K. Rissanen and Elina Sievänen, *Steroidal supramolecular metallogels*. Chem. Soc. Rev. 49, 1977-1998 (2020).
2. P. Terech, M. Yan, M. Maréchal, G. Royal, J. Galveza, S. K. P. Velua, *Characterization of strain recovery and "self-healing" in a self-assembled metallo-gel*. Phys. Chem. Chem. Phys. 15, 7338-7344 (2013).
3. V. Singh, S. Kala, T. Rom, A. K. Paul, R. Pandey, *A multi-cation responsive Ni (ii)-supramolecular metallogel mimics a molecular keypad lock via reversible fluorescence switching*. Dalton Trans. 52, 7088-7103 (2023).
4. K. Kumari et al., *Structural and resistive switching behaviour in lanthanum strontium manganite-reduced graphene oxide nanocomposite system*. J. Alloys Compd. 815, 152213 (2020).
5. K. Kumari et al., *Temperature-dependent resistive switching behaviour of an oxide memristor*. Mater. Lett. 303, 130451 (2021).
6. K. Kumari, A.D. Thakur, S.J. Ray, *The effect of graphene and reduced graphene oxide on the resistive switching behavior of* $La_{0.7}Ba_{0.3}MnO_3$. *Mater*. Today Commun. 26, 102040 (2021).
7. K. Kumari et al., *Charge transport and resistive switching in a 2D hybrid interface. Mater*. Res. Bull. 139, 111195 (2021).
8. S. Majumder, K. Kumari, S.J. Ray, *Pulsed voltage induced resistive switching behavior of copper iodide and* $La_{0.7}Sr_{0.3}MnO_3$ *nanocomposites*. Mater. Lett. 302, 130339 (2021).
9. N. Alam et al., *A wide bandgap semiconducting*

magnesium hydrogel: moisture harvest, iodine sequestration, and resistive switching. Langmuir 38(34), 10601–10610 (2022).
10. K. Kumari et al., *Role of an oxide interface in a resistive switch*. Curr. Appl. Phys. 35, 16–23 (2022).
11. K. Kumari, S.J. Ray, A.D. Thakur, *Resistive switching phenomena: a probe for the tracing of secondary phase in manganite*. Appl. Phys. A 128(5), 430 (2022).
12. K. Kumari, A.D. Thakur, S.J. Ray, *Structural, resistive switching and charge transport behaviour of (1-x)$La_{0.7}Sr_{0.3}MnO_3$. (x) ZnO composite system*. Appl. Phys. A 128(11), 992 (2022).
13. S. Majumder, K. Kumari, S.J. Ray, *Temperature-dependent resistive switching behavior of a hybrid semiconductor-oxide planar system*. Appl. Phys. A 129(5), 1–10 (2023).
14. M. Pedro et al., *Tuning the conductivity of resistive switching devices for electronic synapses. Microelectron*. Eng. 178, 89–92 (2017).
15. D. Ielmini, *Brain-inspired computing with resistive switching memory (RRAM): devices, synapses and neural networks*. Microelectron. Eng. 190, 44–53 (2018).
16. S. Petzold et al., *Forming-free grain Boundary Engineered Hafnium Oxide Resistive Random-Access Memory devices*. Adv. Electron. Mater. 5(10), 1900484 (2019).
17. K. Moon et al., *RRAM-based synapse devices for neuromorphic systems*. Faraday Discuss. 213, 421–451 (2019).
18. J. Choi et al., *Enhanced endurance organolead halide perovskite resistive switching memories operable under an extremely low bending radius*. ACS Appl. Mater. Interfaces. 9(36), 30764–30771 (2017).
19. H. Ma et al., *Interface state-induced negative differential resistance observed in hybrid perovskite resistive switching memory*. ACS Appl. Mater. Interfaces. 10(25), 21755–21763 (2018).
20. J. Han, Su et al., *Lead-free all-inorganic cesium tin iodide perovskite for filamentary and interface-type resistive switching toward environment-friendly and temperature-tolerant nonvolatile memories*. ACS Appl. Mater. Interfaces. 11(8), 8155–8163 (2019).
21. M. Abbasi, Sehar et al., *Biomaterial-induced stable resistive switching mechanism in TiO_2 thin films: the role of active interstitial sites/ions in minimum current leakage and superior bioactivity*. ACS Omega. 5(30), 19050–19060 (2020).
22. B. Sun et al., *An organic nonvolatile resistive switching memory device fabricated with natural pectin from fruit peel*. Org. Electron. 42, 181–186 (2017).
23. A. Kumar et al., *Graphene mediated resistive switching and thermoelectric behavior in lanthanum cobaltate*. J. Appl. Phys. 127, 23 (2020).
24. S. K. Cheung, N. W. Cheung, *Extraction of Schottky diode parameters from forward current-voltage characteristics*. Appl. Phys. Lett. 49, 85-87 (1986).
25. A. Roy, K. Kumari, S. Majumder, S.J. Ray, *Eco-Friendly Biomemristive Nonvolatile Memory: Harnessing Organic Waste for Sustainable Technology*. ACS Applied Bio Materials. 8, 5147-5157 (2024).
26. J. W. Seo, J.-W. Park, K. S. Lim, S. J. Kang, Y. H. Hong, J. H. Yang, L. Fang, G. Y. Sung, H.-K. Kim, *Transparent flexible resistive random access memory fabricated at room temperature*. Appl. Phys. Lett., 95,133508 (2021).
27. M.-C. Wu, J.-Y. Chen, Y.-H. Ting, C.-Y. Huang, W.-W. Wu, *A novel high-performance and energy-efficient RRAM device with multi-functional conducting nanofilaments.* Nano Energy, 82,105717 (2021).
28. X. Ding, Y. Feng, P. Huang, L. Liu, J. Kang, *Low-power resistive switching characteristic in HfO_2/TiO_x bi-layer resistive random-access memory.* Nanoscale Res. Lett., 14, 157 (2019).
29. S. Lee, J. Sohn, Z. Jiang, H.-Y. Chen, H. S. Philip Wong, Metal oxide-resistive memory using graphene-edge electrodes. Nat. Commun., 6, 8407 (2015).
30. Y. J. Huang et al., *Graphene/h-BN heterostructures for vertical architecture of RRAM design.* Sci. Rep., 7, 9679 (2017).